Electronic Supplementary Material (ESI) for Materials Horizons.

— Supplementary Information —

Material Descriptors for Thermoelectric Performance of Narrow-gap Semiconductors and Semimetals

Michael Y. Toriyama,*,† Adam N. Carranco,‡ G. Jeffrey Snyder,† and Prashun Gorai*,‡

†*Materials Science and Engineering, Northwestern University, Evanston, IL 60208, USA.*

‡*Metallurgical and Materials Engineering, Colorado School of Mines, Golden, CO 80401, USA.*

E-mail: MichaelToriyama2024@u.northwestern.edu; pgorai@mines.edu

Material Descriptors

Table S1: Material properties and descriptors of Mg_3Bi_2, Bi_2Te_3, Bi_2Se_3, and Zintl phases calculated with hybrid DFT functional (HSE06). Spin-orbit coupling effects are included. ICSD # is the ICSD number, SG is the space group number, B is the bulk modulus in GPa, E_g is the band gap in eV, $N_{V,VB}$ and $N_{V,CB}$ are the valence and conduction band valley degeneracies, m_h^* and m_e^* are the valence and conduction band effective masses, and B_p and B_n are the p- and n-type TE quality factors. R_B is the asymmetry parameter. zT_{max} is the predicted maximum zT at 300 K. The dominant charge carrier scattering is assumed to be acoustic deformation potential (ADP) or polar optical phonon (POP) scattering.

Compound	ICSD #	SG	B	E_g	$N_{V,VB}$	m_h^*	$N_{V,CB}$	m_e^*	B_p	B_n	R_B	n/p	zT_{max} (ADP)	zT_{max} (POP)
$SrSb_2$	52307	11	33	0.32	3	0.44	4	0.31	0.011	0.018	1.6	n	0.07	0.39
Mg_3Bi_2	659569	164	35	-0.11	1	0.87	6	0.32	0.002	0.021	11.0	n	0.05	0.32
Zn_3As_2	611608	206	56	0.44	2	0.64	3	0.21	0.004	0.012	2.9	n	0.05	0.29
Mg_3Sb_2	2142	164	42	0.55	1	0.63	6	0.43	0.002	0.011	7.6	n	0.05	0.28
Bi_2Te_3	44983	166	31	0.18	6	0.87	2	0.34	0.011	0.006	1.7	p	0.04	0.26
NaCdSb	12159	62	31	0.41	2	0.51	2	0.26	0.006	0.009	1.5	n	0.04	0.23
$CaGa_2As_2$	422526	166	53	0.38	1	0.26	4	0.3	0.002	0.009	3.6	n	0.03	0.22
NaZnSb	12154	129	38	-0.23	8	0.42	1	0.35	0.031	0.004	7.2	p	0.04	0.2
$Li_4Ba_3As_4$	280027	71	35	0.51	3	0.75	1	1.74	0.007	0.001	5.0	p	0.03	0.19
$NaZn_4As_3$	262036	166	75	0.69	1	1.02	4	0.43	0.001	0.007	6.7	n	0.03	0.19
$BaCd_2Sb_2$	32021	164	35	0.27	2	0.31	1	0.65	0.007	0.002	3.1	p	0.03	0.19
$Rb_2Cd_5As_4$	290262	63	35	0.31	2	1.05	1	0.14	0.004	0.007	1.6	n	0.03	0.19
$Ba_3Cd_2Sb_4$	173685	12	30	0.24	2	0.6	1	0.63	0.007	0.003	2.1	p	0.03	0.18
$Ba_2Sn_3Sb_6$	82529	62	27	0.22	2	1.11	2	0.83	0.004	0.005	1.2	n	0.02	0.14

Compound	ICSD #	SG	B	E_g	$N_{V,VB}$	m_h^*	$N_{V,CB}$	m_e^*	B_p	B_n	R_B	n/p	zT_{max} (ADP)	zT_{max} (POP)
Mg_2ZnAs_2	610834	12	17	1.64	1	1.08	3	0.41	0.001	0.004	5.4	n	0.02	0.13
$NaCd_4As_3$	262035	166	32	0.13	2	0.82	1	0.2	0.004	0.004	1.1	n	0.02	0.13
$RbCd_4As_3$	262037	166	32	0.12	1	0.73	1	0.22	0.002	0.004	2.1	n	0.02	0.12
$CaSb_2$	862	11	33	-0.19	3	0.33	4	0.37	0.012	0.015	1.2	n	0.01	0.12
KCd_4As_3	262032	166	31	0.14	1	0.75	1	0.21	0.002	0.004	2.1	n	0.02	0.12
$Ba_5In_2Sb_6$	62305	55	22	0.37	2	0.94	2	1.69	0.004	0.003	1.4	p	0.02	0.12
$BaZn_2Sb_2$	32020	62	38	0.08	1	0.47	1	0.51	0.004	0.004	1.0	p	0.01	0.11
KHgSb	56201	194	15	0.49	1	1.87	1	0.36	0.001	0.004	2.7	n	0.02	0.11
InAs	41993	205	46	0.09	1	0.61	1	0.21	0.002	0.004	1.9	n	0.01	0.11
$BaZn_2As_2$	417000	139	47	0.18	1	0.74	1	0.35	0.002	0.004	1.6	n	0.01	0.11
Bi_2Se_3	42545	166	32	0.32	1	0.51	1	0.3	0.003	0.004	1.4	n	0.01	0.11
$CsZn_4As_3$	262030	123	30	0.47	2	1.14	1	0.99	0.003	0.002	1.8	p	0.01	0.11
$Ca_5Ga_2Sb_6$	36466	55	30	0.36	2	1.38	2	1.96	0.003	0.003	1.2	p	0.01	0.1
TlCdSb	9572	62	33	-0.31	1	0.23	4	0.29	0.007	0.024	3.5	n	0.01	0.1
$BaZn_2P_2$	12145	139	54	0.45	1	0.86	1	0.38	0.002	0.003	1.6	n	0.01	0.09
$RbZn_4As_3$	262038	123	29	0.57	2	1.62	1	1.09	0.003	0.002	1.6	p	0.01	0.09
Cd_3As_2	56167	224	45	-0.47	1	0.5	3	0.13	0.003	0.018	6.8	n	0.02	0.07
$BaSb_2$	409517	11	33	-0.36	1	0.26	2	0.36	0.005	0.008	1.6	n	0.0	0.05

Sensitivity of Thermoelectric Performance to Changes in Band Gap

Table S2: Maximum zT at 300 K (zT_{300K}) for Mg_3Bi_2, Bi_2Te_3 and candidate Zintl phases and change in zT_{300K} to changes in the band gap (E_g). The change in zT_{300K} is shown when E_g changes by 25 meV and 100 meV.

Compound	max. zT_{300K}	change in max. zT_{300K}			
		E_g-25 meV	E_g+25 meV	E_g-100 meV	E_g+100 meV
$SrSb_2$	0.39	-1.6×10^{-6}	3.5×10^{-6}	-2.8×10^{-6}	8.4×10^{-5}
Mg_3Bi_2	0.32	-0.03	0.03	-0.09	0.1
Zn_3As_2	0.29	-1.4×10^{-7}	2.3×10^{-8}	-3.5×10^{-8}	2.6×10^{-7}
Bi_2Te_3	0.26	-4.1×10^{-5}	9.6×10^{-5}	-6.9×10^{-5}	1.9×10^{-3}
NaCdSb	0.23	-8.0×10^{-8}	7.3×10^{-9}	-8.0×10^{-8}	7.7×10^{-7}

Transport Schematic: Acoustic Deformation Potential Scattering

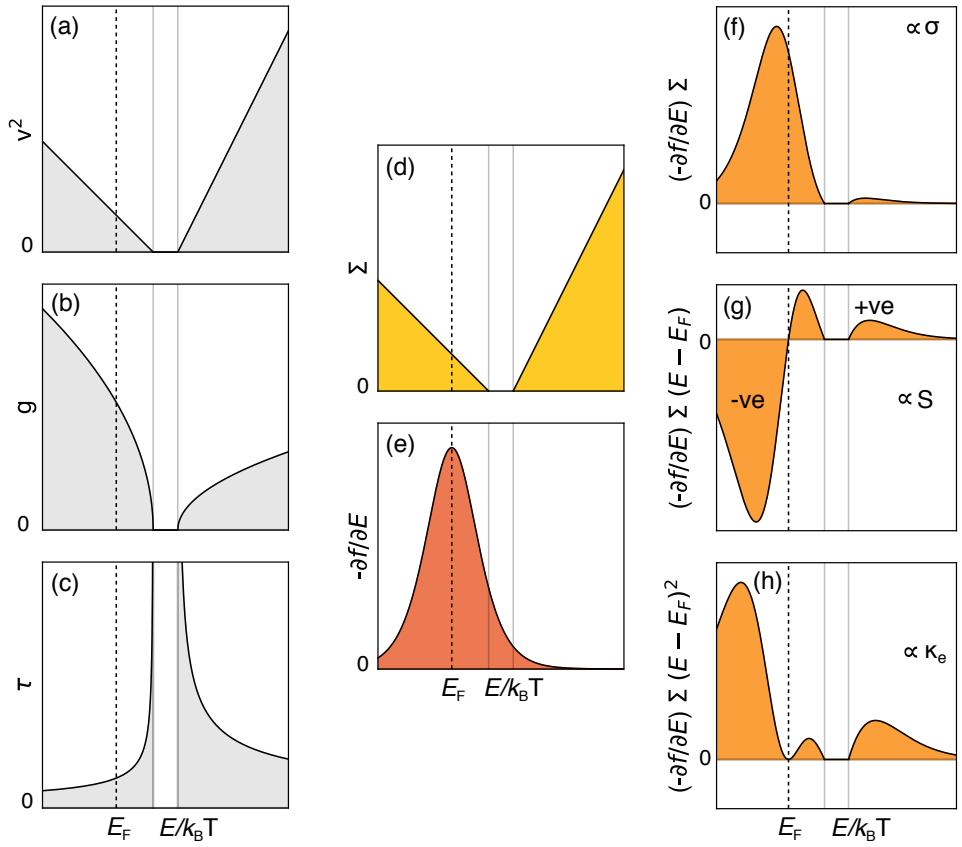

Figure S1: Transport coefficients in a two-band model with valence and conduction bands assuming deformation potential scattering ($r = -1/2$). (a-c) The components of the transport function $\Sigma(E) = v^2(E)g(E)\tau(E)$, shown in (d), where $v(E)$, $g(E)$, and $\tau(E)$ are the energy-dependent velocity, density of states, and scattering time, respectively. $\Sigma(E)$ is sampled by the selection function $-\partial f/\partial E$, shown in (e), and weighted by $(E - E_\mathrm{F})^m$ to obtain (f) the electrical conductivity σ ($m = 0$), (g) Seebeck coefficient S ($m = 1$), and (h) the Lorenz number ($m = 2$), which is related to the electronic thermal conductivity. The area under the curves are proportional to the magnitude of each transport coefficient.

$zT_{300\mathrm{K}}$ for Acoustic Deformation Potential Scattering

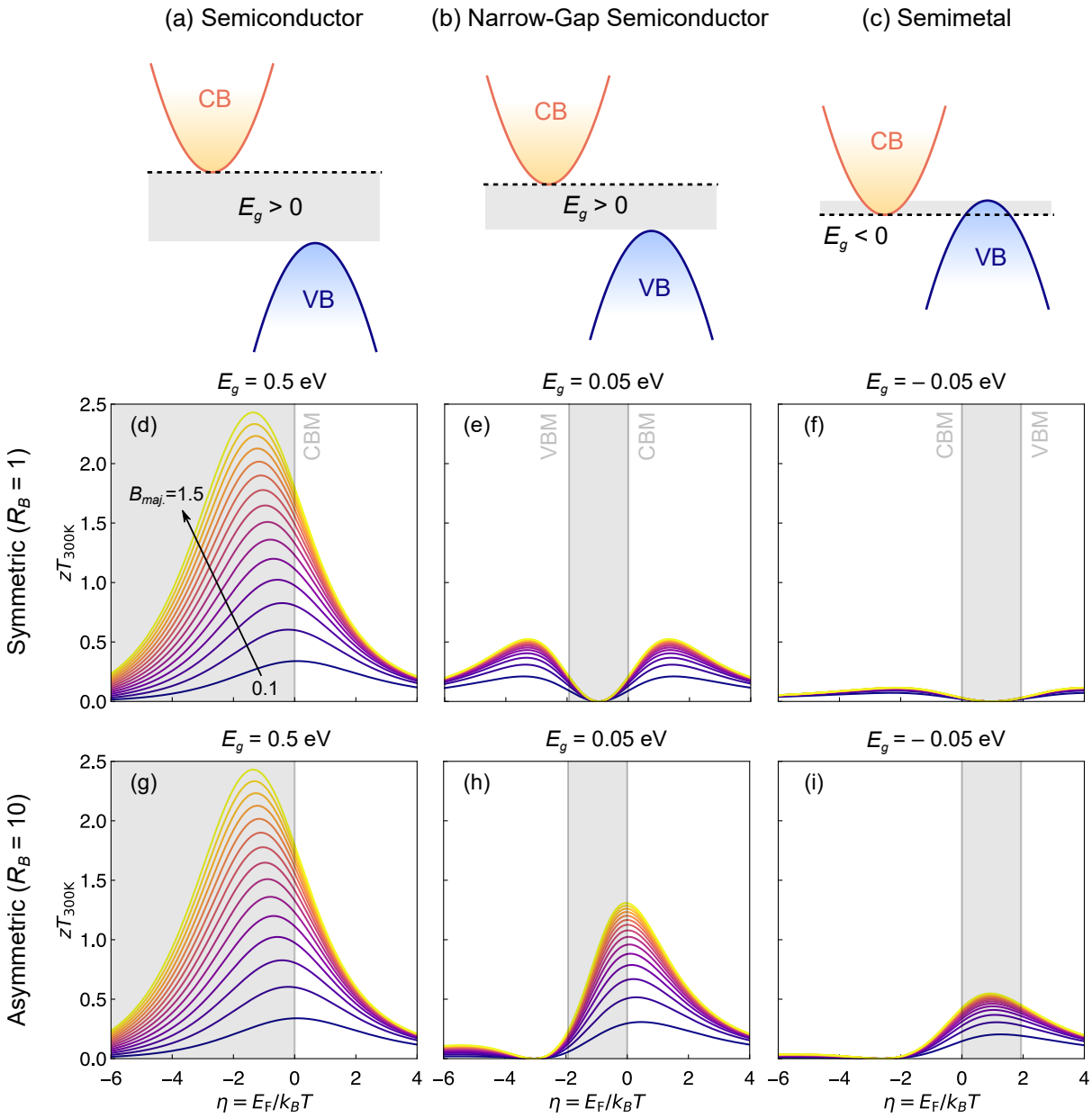

Figure S2: zT as a function of the reduced Fermi energy (η) for (a) semiconductors, (b) narrow-gap semiconductors, and (c) semimetals. The zT vs. η curves are plotted at 300 K assuming deformation potential scattering ($r = -1/2$) for different values of $B_{\mathrm{maj.}}$, ranging from $B_{\mathrm{maj.}} = 0.01$ (dark blue) to $B_{\mathrm{maj.}} = 1.5$ (yellow). Panels (d) – (f) are drawn for the symmetric ($R_B = 1$) case. Panels (g) – (i) illustrate the asymmetric case ($R_B = 10$).

Transport Parameters: Acoustic Deformation Potential Scattering

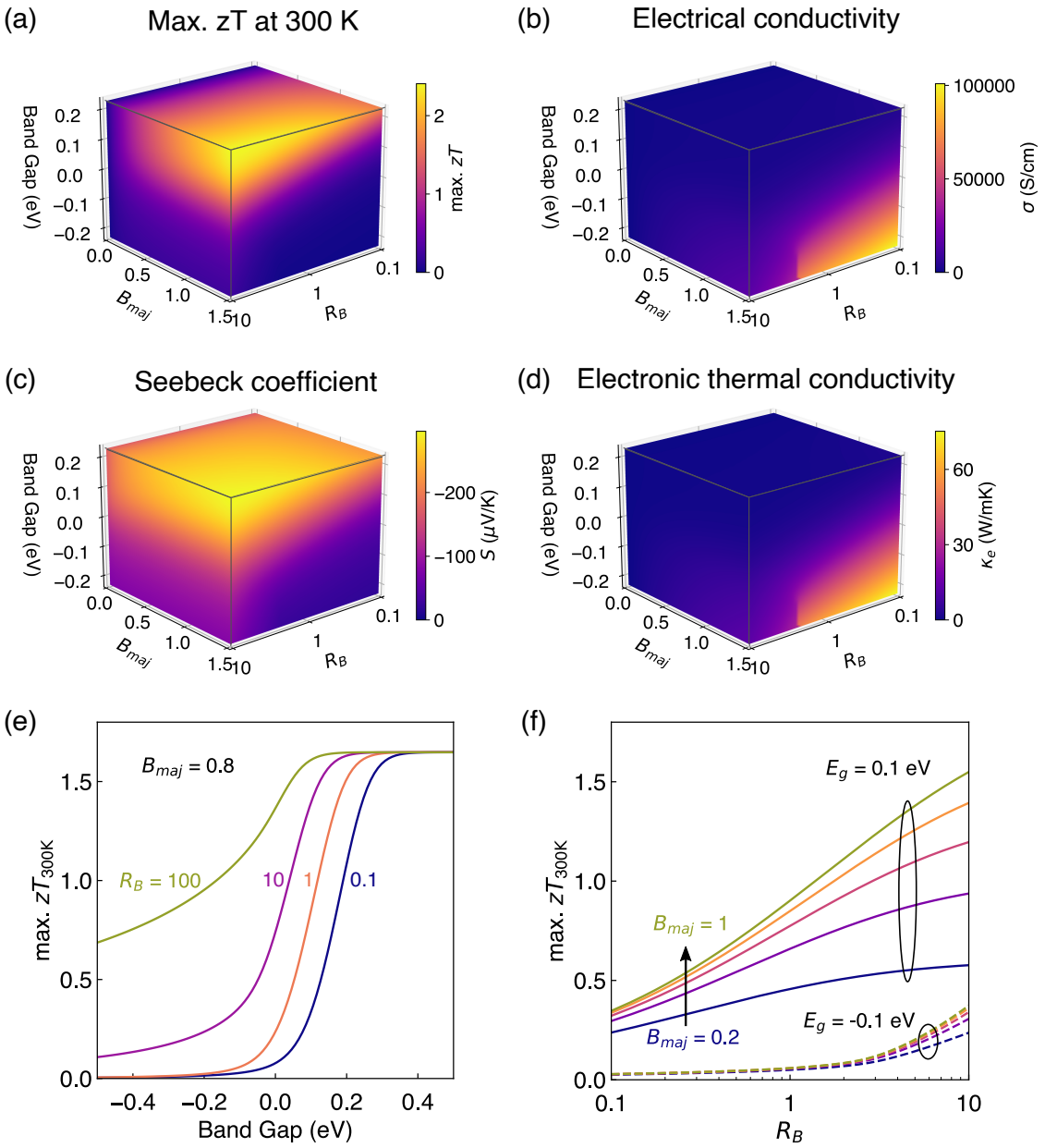

Figure S3: (a) Maximum zT at 300 K as a function of band gap E_g, quality factor of majority carriers B_{maj}, and asymmetry parameter $R_B = B_{maj}/B_{min}$. Deformation potential scattering ($r = -1/2$) is assumed. The electrical conductivity (b), Seebeck coefficient (c), and electronic thermal conductivity (d) are shown at the E_F where zT is maximized at 300 K. (e) Maximum zT at 300 K as a function of band gap, assuming $B_{maj} = 0.8$. Each curve corresponds to a different R_B value. (f) Maximum zT at 300 K for different R_B values, shown for $E_g = 0.1$ eV and $E_g = -0.1$ eV. Each curve corresponds to a different B_{maj}. Wide-gap materials exhibit high zT; however, high performance can also be achieved in narrow-gap semiconductors and semimetals with high B_{maj} and R_B.

Specific Case of $R_B < 1$

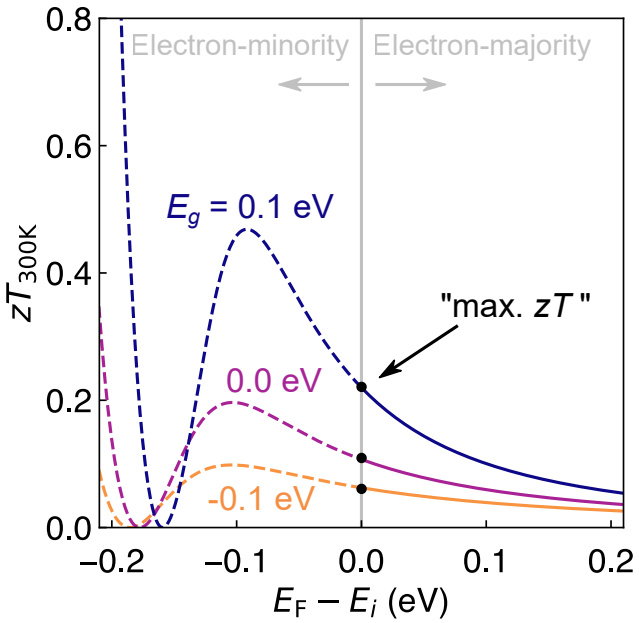

Figure S4: Illustration of the maximum zT when $R_B < 1$ for different band gap (E_g) values. Here, we assign electrons as the majority carriers, and set $R_B = 0.01$ and $B_{maj} = 0.8$. E_i is the intrinsic Fermi level, where $E_F > E_i$ implies that electrons are the majority carriers. Since electrons are assumed to be the majority carriers, the "maximum zT" is determined to be the zT when $E_F = E_i$ despite not being the true maximum.

Quality Factor for Single-Band Transport

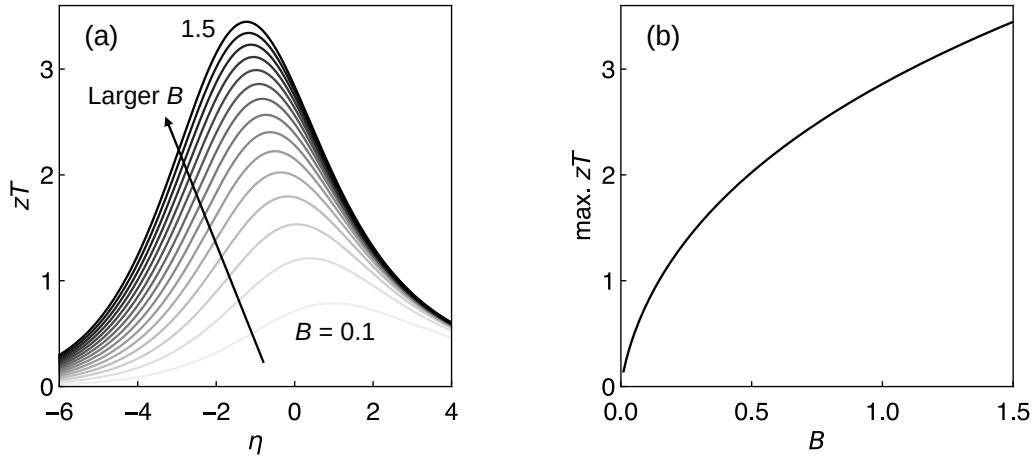

Figure S5: (a) zT vs. doping assuming single-band transport, for different values of the quality factor B. The quality factor increases from the lighter to darker curve. (b) The maximum zT plotted against B. In a system where transport can be described using a single parabolic band, the quality factor B monotonically increases with the maximum attainable zT.

Material parameter B_{bp} for Different Scattering Mechanisms

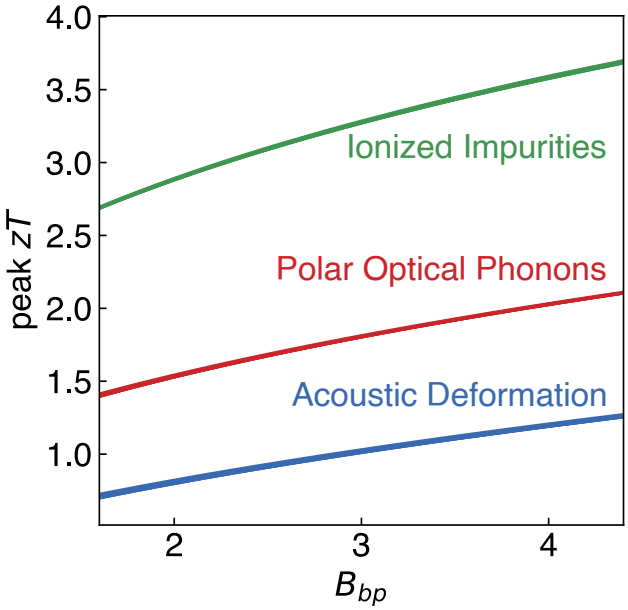

Figure S6: Peak zT plotted against material parameter B_{bp} for different scattering mechanisms: acoustic deformation potential (blue, $r = -1/2$), polar optical phonons (red, $r = 1/2$), and ionized impurities (green, $r = 3/2$). We consider R_B values ranging between 0.125 and 8, as in the main text. n is set to 1.16.

Calculated B_{bp} of Zintl Phases

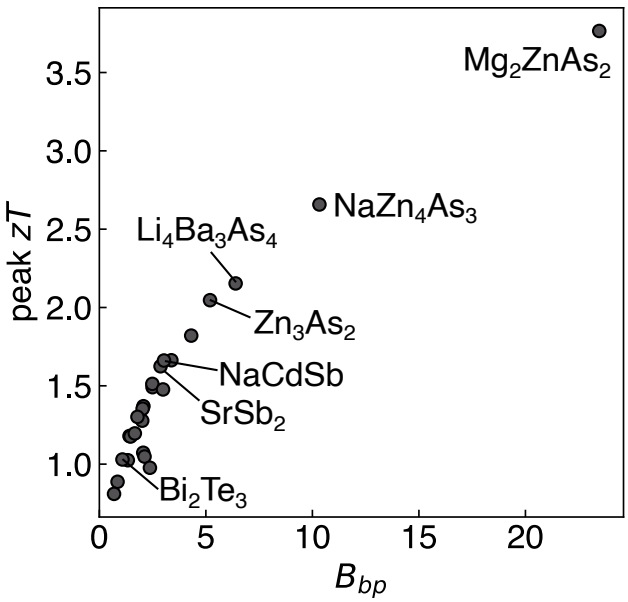

Figure S7: Peak zT plotted against B_{bp} for narrow-gap Zintl phases considered in this study. Scattering by polar optical phonons is assumed. In addition to the three phases found to be promising TEs at room temperature ($SrSb_2$, Zn_3As_2, and NaCdSb), we find other phases that exhibit potentially higher peak zT (Mg_2ZnAs_2, $NaZn_4As_3$, and $Li_4Ba_3As_4$).

Schematic Electronic Band Structures with Different R

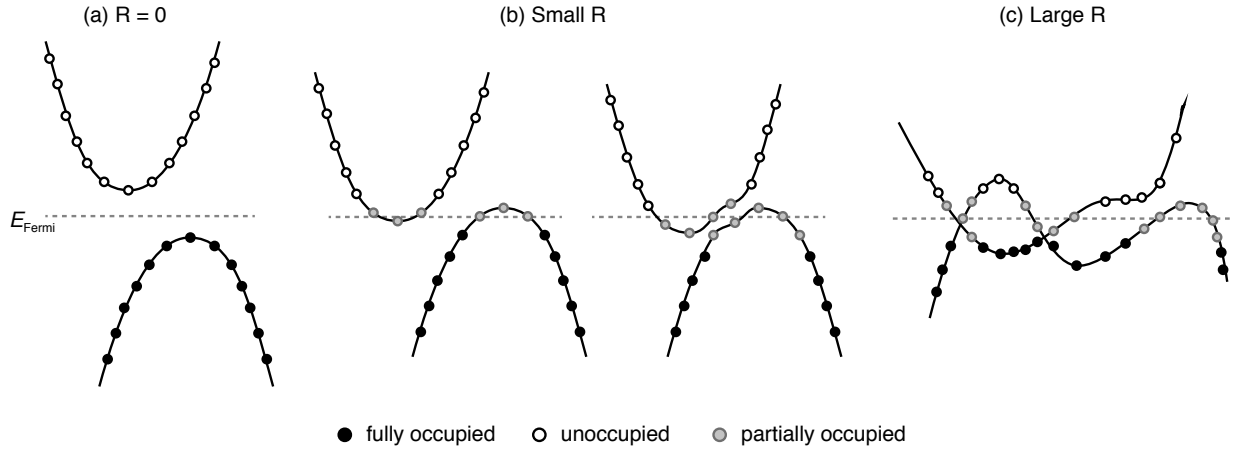

Figure S8: Schematic electronic band structures representing three different values of R (see Eq. 19): (a) $R = 0$ represents a semiconductor/insulator, where $O_{n,k}$ is either 2 or 0 (assuming doubly occupied bands), (b) small R represents a semimetal, where $O_{n,k}$ is fractional at a few k-points relative to the total number of k-points sampled, and (c) large R represents a metal where $O_{n,k}$ is fractional at many k-points. $O_{n,k}$ is the occupation of band index n at a k-point. The horizontal dotted line is the Fermi level (E_{Fermi}).